Chemical Science

ROYAL SOCIETY OF CHEMISTRY

EDGE ARTICLE

Cite this: *Chem. Sci.*, 2020, **11**, 2770

All publication charges for this article have been paid for by the Royal Society of Chemistry

Received 18th October 2019
Accepted 4th February 2020

DOI: 10.1039/c9sc05268b

rsc.li/chemical-science

Probing a variation of the inverse-trans-influence in americium and lanthanide tribromide tris(tricyclohexylphosphine oxide) complexes†

Cory J. Windorff, Cristian Celis-Barros, Joseph M. Sperling, Noah C. McKinnon and Thomas E. Albrecht-Schmitt *

The synthesis, characterization, and theoretical analysis of meridional americium tribromide tris(tricyclohexylphosphine oxide), *mer*-$AmBr_3(OPcy_3)_3$, has been achieved and is compared with its early lanthanide (La to Nd) analogs. The data show that homo *trans* ligands display significantly shorter bonds than the *cis* or hetero *trans* ligands. This is particularly pronounced in the americium compound. DFT along with multiconfigurational CASSCF calculations show that the contraction of the bonds relates qualitatively with overall covalency, *i.e.* americium shows the most covalent interactions compared to lanthanides. However, the involvement of the 5p and 6p shells in bonding follows a different order, namely cerium > neodymium ~ americium. This study provides further insight into the mechanisms by which ITI operates in low-valent f-block complexes.

Introduction

Phosphine oxides are highly stable ligands that have been utilized primarily for catalysis on elements across the periodic table.[1] The study of phosphine oxides with f-elements has primarily focused on their use in extraction processes[2–5] and in (pseudo)halide/nitrate f-element starting materials.[6–9] The effect of two ligands *trans* to one another is most prototypically examined in the actinyls, AnO_2^{n+}, where the *trans*-oxygens display unusually short bond distances and high bond strength, best described as bond order of three.[10] This effect, termed the inverse-trans-influence (ITI) as a general concept has become the focus of several experimental and theoretical investigations and has evolved to be primarily applied to ligands *trans* to multiply bonded ligands.[11–17] This has also been studied in the $[AnOX_5]^{n-}$ complexes (An = Pa^V, U^{VI}, X = F, Cl, Br),[18,19] where reaction of HBr with $[UOCl_5]^{1-}$ yields $[UO(Cl)Br_4]^{1-}$ where all of the equatorial Cl's have been replaced by Br's, but the *trans*-Cl is retained, which also possess the shortest M–Cl bond in the molecule.[19] These seminal studies helped to show that something was unusual with high valent actinides where a ligand was *trans* to an oxo ligand, though these studies have not been revisited with modern instrumentation and methods. A prototypical examination on the effect of ITI is through the use of meridional octahedral compounds, *e.g.* *mer*-MX_3L_3, Fig. 1, which has been thoroughly studied in the transition metal series, but is significantly less studied in the f-block.[20] However, the primary focus of structural and theoretical studies on actinide molecules displaying the ITI effect have been focused on high valent, +4 to +6, oxidation states.[13,21–25] Lanthanides have only been subjected to structural studies in the +3 oxidation state,[12,26] with some analysis of Ce(IV) and hypothetical Pr(IV) and Tb(IV) molecules.[15,17] In this study on a variation of the ITI we are relying on a hole being created in 5/6p-orbitals of a low valent f-element complex without substantive multiple bond character in the *trans* ligand. The amount of ITI can be quantified as a percentage that implies that the lower the percentage value the larger the ITI effect, eqn (1), where r = bond distance, M = metal, X = neutral or anionic ligand.[27] Herein, we base our discussion from the most basic and general definition given in the literature by Denning as the polarization of the core electrons towards the f shell driven by a tightly bound ligand.

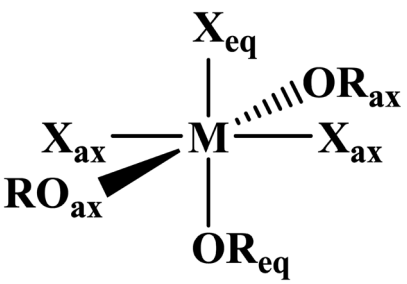

Fig. 1 General depiction of ligand designations in *mer*-MX_3L_3.

Department of Chemistry and Biochemistry, Florida State University, 95 Chieftan Way, RM. 118 DLC, Tallahassee, Florida 32306, USA. E-mail: talbrechtschmitt@fsu.edu

† Electronic supplementary information (ESI) available: Photographs of compounds, NMR spectra, electronic absorption spectra, additional theoretical calculation. CCDC 1959746–1959750. For ESI and crystallographic data in CIF or other electronic format see DOI: 10.1039/c9sc05268b

Because these orbitals are lower in energy in the valence region.[28] This effect produces an electron deficiency in the position *trans* to the polarizing ligand that is compensated by a secondary ligand. This broad and perhaps oversimplified definition of ITI represents a solid basis without the need to assume any oxidations state or ligands.

$$\mathrm{ITI} = \frac{r(\mathrm{M}-\mathrm{X}_{trans})}{r(\mathrm{M}-\mathrm{X}_{cis})} \times 100 \quad (1)$$

The minor actinides, Am and Cm, contribute high levels of radiation and heat in spent nuclear fuel. Long-lived isotopes of Am [^{241}Am ($t_{1/2}$ = 432 years), ^{243}Am ($t_{1/2}$ = 7370 years)] can be transmuted into radionuclides with a much shorter-half life, which is important for the end of the nuclear fuel cycle. However, the separation of these minor actinides from other fission products, such as lanthanides, remains a difficult problem. The additional separation of Am^{III}/Cm^{III} is a great challenge due to their similar chemical properties and ionic radii. Phosphine oxide ligands have recently demonstrated relatively high selectivity for the Am–Cm pair in the form of $(Ph_2PyPO)_2M(NO_3)_3$.[29] Although phosphine oxides are heavily utilized in separation of f-elements relevant to the nuclear fuel cycle, there have been few crystallographic studies for *trans*-uranium elements, and indeed only the mono and bis [Opy-2,6-$CH_2(Ph)_2PO$], **NOPOPO**, adducts have been reported.[30] Herein we examine the synthesis and structure in saturated tricyclohexylphosphine oxide adducts of f-element tribromides, and the effects of the ITI on trivalent f-elements.

Experimental details

General considerations

Caution! ^{243}Am ($t_{1/2}$ = 7364 years) and its daughters have high specific activity α-particle and, γ emitting radionuclides, and its use presents extreme hazards to human health. This research was conducted in radiological and nuclear facilities with appropriate analyses of these hazards and implementation of controls for the safe handling and manipulation of these toxic and radioactive materials.

Materials

All experiments were conducted in air with no attempt to exclude air or water. Reagents and solvents, $OPcy_3$ (cy = cyclohexyl, C_6H_{11}, Alfa Aesar), $CDCl_3$, CD_2Cl_2, CD_3OD, (Cambridge), ^{i}PrOH, MeOH, DCM (Sigma) $NH_{3(aq)}$ (Baker) were purchased from commercial sources and used as received. $LnBr_3 \cdot 6H_2O$ (Ln = La–Nd) were synthesized by dissolution of Ln_2O_3 in concentrated $HBr_{(aq)}$ and heated at 150 °C in a box furnace until viscous, then agitated, stirred until cooled to room temperature, dissolved in water and evaporated to a residue. This process was repeated twice. The product was washed with ether, to remove residual acid and Br_2, until washings were colorless, dried under house vacuum for 10–15 min and stored in a desiccator and used with the assumed hydration number of six. All ^{243}Am synthetic manipulations were performed in a certified chemical fume hood, and a known concentration stock solution was prepared as previously described.[31] Aqueous manipulations were performed with >18 Ω water from a Millipore purification system.

Instrumentation

^{1}H, $^{13}C\{^{1}H\}$ and $^{31}P\{^{1}H\}$ NMR spectra were recorded at 298(2) K on a Bruker 600 MHz NMR spectrometer operating at 600.13, 150.90, and 242.94 MHz, respectively, low temperature ^{1}H and $^{31}P\{^{1}H\}$ spectra were recorded on a Varian Inova 500 MHz spectrometer at 187 K operating at 499.80, 202.34 MHz, respectively, for all lanthanide samples. The sample of $^{243}AmBr_3(OPcy_3)_3$ was recorded at 295(2) K on a Bruker 400 MHz NMR spectrometer operating at 400.17, 100.62, and 161.99 MHz, respectively. ^{1}H and $^{13}C\{^{1}H\}$ were referenced to internal solvent resonances, $^{31}P\{^{1}H\}$ spectra were referenced externally to 85% H_3PO_4. For radiologic containment, $^{243}AmBr_3(OPcy_3)_3$ was dissolved in minimal $CDCl_3$, transferred to a PTFE NMR tube liner, sealed, checked for contamination, placed inside a high quality borosilicate NMR tube, and checked again for contamination before being transported to the spectrometer. Due to the paramagnetism of Am^{3+}, Ce^{3+}, Pr^{3+} and Nd^{3+}, and in particular the small sample size of $^{243}AmBr_3(OPcy_3)_3$, only unambiguously identifiable peaks are assigned. For clarity all paramagnetic $^{13}C\{^{1}H\}$ and $^{31}P\{^{1}H\}$ spectra were processed with a 5 and 10 Hz line broadening, respectively. High resolution mass-spectra were recorded on an Agilent 6200 Q-TOF-MS coupled to a DART SVP (IonSense) ambient ionization source. All analyses were conducted in positive mode with a DART helium gas at 350 °C, Q-TOF heater gas (He) at 300 °C, drying gas flow at 0.2 L min^{-1}, fragmentor voltage 175 V, skimmer voltage 65 V, and a mass range of 100–1700 amu with high resolution. Solution phase UV/vis/NIR measurements were made on an Agilent Technologies Cary 6000i UV/vis/NIR spectrophotometer in 1.0 cm small volume quartz cells between 200 to 1400 nm (methanol) or 235 to 1000 nm (DCM), at a resolution of 0.1 nm. Single crystal UV/vis/NIR measurements were recorded on crystals in immersion oil® placed on a glass slide and recorded using a CRAIC microphotospectrometer from 320 to 1700 nm. Single crystals of the lanthanide complexes were mounted on nylon cryoloops with Paratone-N oil. Crystals of $^{243}AmBr_3(OPcy_3)_3$ was mounted with appropriate layers of containment. Crystallographic data from all single crystals were collected on a Bruker D8 Quest diffractometer with a Photon 100 complementary metal-oxide-semiconductor (CMOS) detector, and cooled to 120(2) or 130(2) K using an Oxford Cryostream or CRYO Industries low-temperature device. The instrument was equipped with graphite monochromatized Mo K_α X-ray source (λ = 0.71073 Å). The APEX3 (ref. 32) program package was used to determine the unit-cell parameters and for data collection. The raw frame data was processed using SAINT[33] and SADABS[34] to yield the reflection data file. Subsequent calculations were carried out using the SHELXTL[35,36] or OLEX2 (ref. 37) programs.

Theoretical methods

The coordinates of $MBr_3(OPcy_3)_3$ (M = Am, Ce, Nd) for the calculations were obtained directly from the crystal structure to

keep the constraints imposed by the solid-state packing. To utilize multiconfigurational calculations, the complete active space self-consistent field (CASSCF) approximation[38] was used as implemented in the ORCA 4.1.1 program.[39] Wave functions were obtained utilizing the SARC-TZVP basis set for the metal centers and the Def2-TZVP basis functions for the rest of the atoms. The active space considered were n electrons ($n = 1$, 3, 6 for Ce, Nd, and Am) in the seven f orbitals giving rise to a CAS(n,7). Scalar relativistic effects were included by the second-order Douglas–Kroll–Hess (DKH2) Hamiltonian. State interactions *via* quasi-degenerate perturbation theory (QDPT) were used to correct the wave function for spin–orbit coupling (SOC). The resulting wave functions (SO-CAS) were used to analyze the nature of the ground and low-lying excited states, whereas the scalar relativistic wave functions (SR-CAS) were used for further bonding analysis.

The nature of the chemical bonds was addressed performing a topological analysis of the electron density using Bader's quantum theory of atoms in molecules (QTAIM) analysis. Key elements within QTAIM were extracted such as the electron density, delocalization indices, and energy densities at the interatomic region (bond critical point, BCP) which have been employed previously for this aim.[40–48] The covalency was analyzed, on one hand, by changes in the concentration of the electron density at the BCP along with changes in the delocalization indices. On the other hand, energy densities show the polarization of the covalent bond by looking at the ratios between potential [$V(r)$] and kinetic [$G(r)$] energy densities, which for partial covalent bonds lie in between values of 1 and 2. The total energy density shows the degree of covalency that is represented by the level of predominance of the potential over the kinetic energy density.[49]

A model system was also investigated where the cyclohexyl groups were replaced by methyl groups to simplify the molecular orbital energy diagram picture and allow the observations between the Am, Ce and Nd complexes to be made. The methyl groups were re-optimized while the rest of the molecule was kept frozen to conserve the crystallographic geometry surrounding the metal atom. These calculations were performed in the ADF2019 suite[50,51] using the PBE functional along with the TZP basis set. Frozen-core and all-electron calculations were performed for the full structure to prove the role of 5/6p orbitals in the stabilization of the complexes at the same level of theory. For the frozen-core calculations only core orbitals of metal centers were frozen, *i.e.* up to 5p for lanthanides and 6p for americium. In the particular case of Am, the frozen-core basis set was manually created with support from the ADF developers because it is not available in ADF2019. Furthermore, all-electron geometry optimizations were performed in the model system to confirm that geometries observed experimentally are not imposed by either crystal packing or steric hindrance, see Table S2†. Additionally, ligand-field DFT[52,53] was used to examine the reduction of the inter-electronic repulsion within the 5/6p shell due to central-field and symmetry-restricted covalency. The procedure used herein has been previously described for Cs_2KYF_6:Pr^{3+},[52] where occupation numbers in the f-shell were allowed to be fractional. The reductions were obtained not only with respect to the free ions but also compared to the nona-aquo complexes, $[M(H_2O)_9]^{3+}$, where the geometries were taken from the crystallographic data in the literature.[54–56]

Synthesis of $^{243}AmBr_3(OPcy_3)_3$

An aliquot of ^{243}Am (3.0 mg, 12 μmol) was drawn from a 2 M HCl stock solution and precipitated with excess $NH_{3(aq)}$ to give a pale yellow solid naïvely formulated as "$^{243}Am(OH)_3$", washed with water (2 × 2 mL), suspended in water (∼1 mL) and dissolved with $HBr_{(aq)}$ (concentrated, ∼0.5 mL) to give a yellow solution. The yellow solution was transferred to a 20 mL scintillation vial, placed under a heat lamp and gently evaporated to a yellow residue formulated as $^{243}AmBr_3 \cdot nH_2O$. The residue was dissolved in ^{i}PrOH (1.50 mL) to give a dark yellow solution. A colorless solution of $OPcy_3$ (11 mg, 38 μmol) in ^{i}PrOH (1.00 mL) was added to the ^{243}Am solution, which quickly became turbid and clear again. The solution was capped and left to stand undisturbed. Over 3 h amber colored X-ray quality crystals were deposited. A small sample was withdrawn for spectroscopy (single crystal X-ray diffraction and solid state UV/vis/NIR). The solution was capped and left to stand for 3 days to allow further crystallization. The mother liquor was decanted, washed with Et_2O (3 × 0.5 mL), dried in air and transferred to a glovebox dedicated to actinide chemistry to give **$^{243}AmBr_3(OPcy_3)_3$** as a yellow/brown crystalline solid, 9.0 mg, 54%. ^{1}H NMR ($CDCl_3$; 400 MHz, 295 K) δ: 1.80 (br, s, *cy*), 1.67 (br, s, *cy*), 1.39 (br, s, *cy*), 1.14 (br, s, *cy*); $^{13}C\{^1H\}$ NMR ($CDCl_3$; 101 MHz, 295 K) δ: 27.08 ($^2J_{PC} = 27$ Hz, *cy*), 26.15 (*cy*) 25.90 (*cy*); $^{31}P\{^1H\}$ NMR ($CDCl_3$; 162 MHz, 295 K) δ: 108.89 (s, $\nu_{1/2} = 141$ Hz). Due to the weak paramagnetism and small sample size ^{1}H integration is ambiguous and ^{1}H and $^{13}C\{^1H\}$ peak assignments are tentative, see ESI.† UV/vis/NIR [λ_{max}, nm [cm^{-1}], single crystal]: 340.0 nm [29 411] charge transfer, 368.4 [27 148] $^5G_{2'}$, 380.9 [26 252] $^5G_{4'}$, 433.4 [23 074] $^5H_{4'}$, 457.5 [21 856] $^5G_{2'}$, 477.0 [20 695] $^5D_{2'}$, 508.0 [19 685] $^5L_{6'}$, 524.2 [19 075] $^5L_{6'}$, 777.4 [12 863] $^7F_{6'}$, 805.8 [12 422] $^7F_{6'}$, 823.2 [12 147] $^7F_{6'}$, 1042.6 [9591] $^7F_{4'}$.

General synthesis of $LnBr_3(OPcy_3)_3$, (Ln = La, Ce, Pr, Nd)

As an alternative to the literature[57] a colorless solution of $OPcy_3$ (18 mg, 61 μmol) in ^{i}PrOH (1.0 mL) was added to a yellow solution of $LnBr_3 \cdot 6H_2O$ (∼10 mg, ∼20 μmol) in ^{i}PrOH (1.5 mL) causing the solution to become turbid and then clear. The vial was capped and left to stand overnight during which colorless (La, Pr, Nd) or orange (Ce) X-ray quality crystals were deposited. A small sample was withdrawn for spectroscopy (single crystal X-ray diffraction and solid state UV/vis/NIR). The mother liquor was decanted, washed with Et_2O (3 × 0.5 mL), dried in air and briefly dried under reduced pressure (house vacuum) to give **$LnBr_3(OPcy_3)_3$** as a crystalline solid.

$LaBr_3(OPcy_3)_3$

Colorless **$LaBr_3(OPcy_3)_3$** 20 mg, 80%. ^{1}H NMR ($CDCl_3$; 600 MHz, 298 K) δ: 2.068 (m, 8H, *cy*), 1.991 (m, 18H, *cy*), 1.842 (m, 18H, *cy*), 1.700 (m, 9H, *cy*), 1.600 (m, 18H, *cy*), 1.352–1.261 (m, 28H, *cy*); ^{1}H NMR (CD_2Cl_2; 600 MHz, 298 K) δ: 2.095 (m, 9H, *cy*), 1.989 (s,

18H, *cy*), 1.853 (m, 18H, *cy*), 1.714 (m, 9H, *cy*), 1.661 (m, 18H, *cy*), 1.386–1.282 (m, 28H, *cy*); ^{1}H NMR (CD_2Cl_2; 500 MHz, 187 K) δ: 1.999 (s, 6H, *cy*), 1.849 (s, 15H, *cy*), 1.750 (s 26H, *cy*), 1.563 (m, 24H, *cy*), 1.199 (m, 33H, *cy*); ^{1}H NMR (MeOD-d_4; 600 MHz, 298 K) δ: 2.021 (m, 9H, *cy*), 1.941 (m, 18H, *cy*), 1.861 (m, 18H, *cy*), 1.760 (s, 9H, *cy*), 1.475 (m, 18H, *cy*), 1.372–1.295 (m, 28H, *cy*); ^{1}H NMR (MeOD-d_4; 500 MHz, 187 K) δ: 2.050 (m, 9H, *cy*), 1.871 (m, 36H, *cy*), 1.861 (m, 18H, *cy*), 1.753 (m, 9H, *cy*), 1.428–1.304 (m, 46H, *cy*); ^{13}C{^{1}H} NMR ($CDCl_3$; 151 MHz, 298 K) δ: 34.772 ($^{1}J_{CP}$ = 34.8 Hz, *i-cy*), 26.893 ($^{2}J_{CP}$ = 26.94 Hz, *cy*), 25.996 (*cy*), 25.901 (*cy*); ^{13}C{^{1}H} NMR (CD_2Cl_2; 151 MHz, 298 K) δ: 36.893 ($^{1}J_{CP}$ = 37.0 Hz, *i-cy*), 29.243 ($^{2}J_{CP}$ = 29.2 Hz, *cy*), 28.161 (*cy*); ^{13}C{^{1}H} NMR (MeOD-d_4; 151 MHz, 298 K) δ: 31.061 ($^{1}J_{CP}$ = 36.1 Hz, *i-cy*), 27.736 ($^{2}J_{CP}$ = 27.74 Hz, *cy*), 27.170 (*cy*), 27.055 (*cy*); ^{31}P{^{1}H} NMR ($CDCl_3$; 243 MHz, 298 K) δ: 60.314 (s, O*P*); ^{31}P{^{1}H} NMR (CD_2Cl_2; 243 MHz, 298 K) δ: 60.483 (s, O*P*), ^{31}P{^{1}H} NMR (CD_2Cl_2; 202 MHz, 187 K) δ: 62.216 (s, 4P, O*P*), 61.770 (s, 4P, O*P*), 61.280 (s, 2P, O*P*), 60.865 (s, br, 9P, O*P*); ^{31}P{^{1}H} NMR (MeOD-d_4; 243 MHz, 298 K) δ: 57.209 (s, O*P*), ^{31}P{^{1}H} NMR (MeOD-d_4; 202 MHz, 187 K) δ: 57.192 (s, O*P*). UV/vis/NIR [MeOH, λ_{max}, nm (ε, M^{-1} cm^{-1})]: 209.6 (870), 268.5 (170).

$CeBr_3(OPcy_3)_3$

Orange **$CeBr_3(OPcy_3)_3$** 20 mg, 75%. ^{1}H NMR ($CDCl_3$; 600 MHz, 298 K) δ: 5.29 (br, s, 9H, *cy*), 3.64 (br, s, 18H, *cy*), 2.68 (br, s, 18H, *cy*), 2.01 (s, 18H, *cy*), 1.82 (s, 25H, *cy*), 1.22 (br, s, 10H, *cy*); ^{1}H NMR (CD_2Cl_2; 600 MHz, 298 K) δ: 4.94 (br, s, 9H, *cy*), 3.45 (br, s, 18H, *cy*), 2.53 (br, s, 18H, *cy*), 1.96 (s, 20H, *cy*), 1.77 (s, 26H, *cy*), 1.22 (br, s, 9H, *cy*); (CD_2Cl_2; 500 MHz, 187 K)[58] δ: 12.74, 9.93, 6.94, 4.70, 3.71, 3.39, 2.76, 2.12, 1.90, 1.28, 0.17, −0.48, −1.32, −2.02, −5.20; ^{1}H NMR (MeOD-d_4; 600 MHz, 298 K) δ: 1.37 (br, s, 9H, *cy*), 0.86 (br, s, 18H, *cy*), 0.39, 0.34, 0.33 (br, m, 36H, *cy*), 0.20 (m, 10H, *cy*), 0.11 (m, 26H, *cy*), −0.24 (br, m, 10H, *cy*); ^{1}H (MeOD-d_4; 500 MHz, 187 K) δ: 2.04 (br, s, 9H, *cy*), 1.87 (br, s, 32H, *cy*), 2.68 (br, s, 18H, *cy*), 2.01 (s, 18H, *cy*), 1.82 (s, 25H, *cy*), 1.22 (br, s, 10H, *cy*); ^{13}C{^{1}H} NMR ($CDCl_3$; 151 MHz) δ: 38.76 ($^{1}J_{CP}$ = 38.8 Hz, *i-cy*), 27.51 (*cy*), 26.06 (*cy*); ^{13}C{^{1}H} NMR (CD_2Cl_2; 151 MHz, 298 K) δ: 40.77 ($^{1}J_{CP}$ = 40.8 Hz, *i-cy*), 29.75 ($^{2}J_{CP}$ = 29.7 Hz, *cy*), 29.52 (*cy*), 28.33 (*cy*); ^{13}C{^{1}H} NMR (MeOD-d_4; 151 MHz, 298 K) δ: 39.42 ($^{1}J_{CP}$ = 37.6 Hz, *i-cy*), 28.00 ($^{2}J_{CP}$ = 28.0 Hz, *cy*), 27.85 (*cy*), 27.20 (*cy*); ^{31}P{^{1}H} NMR ($CDCl_3$; 243 MHz) δ: 109.48 (s, O*P*); ^{31}P{^{1}H} NMR (CD_2Cl_2; 243 MHz, 298 K) δ: 107.70 (s, O*P*), ^{31}P{^{1}H} NMR (CD_2Cl_2; 202 MHz, 187 K) δ: 134.28 (s, 1P, O*P*), 118.82 (s, 3P, O*P*), 113.90 (s, 2P, O*P*); ^{31}P{^{1}H} NMR (MeOD-d_4; 243 MHz, 298 K) δ: 69.36 (s, O*P*), ^{31}P{^{1}H} NMR (MeOD-d_4; 202 MHz, 187 K) δ: 57.16 (s, O*P*). UV/vis/NIR [λ_{max}, nm, single crystal]: 339; [DCM, λ_{max}, nm (ε, M^{-1} cm^{-1})]: 326.6 (1160); [MeOH, λ_{max}, nm (ε, M^{-1} cm^{-1})]: 209.1 (1020), 231.6 (250), 252.7 (340), 314.9 (620). DART-MS (*m*/*z*, relative abundance, %) = 1188.34 (100), 1190.34 (61), 1189.34 (58), 1186.34 (52), 1191.34 (31), 1187.345 (29) $[CeBr_2(OPcy_3)_3]^+$.

$PrBr_3(OPcy_3)_3$

Colorless **$PrBr_3(OPcy_3)_3$** 22 mg, 83%. ^{1}H NMR ($CDCl_3$; 600 MHz, 298 K) δ: 20.85 (br, s, $\nu_{1/2}$ = 1470 Hz, 5H, *cy*), 13.55 (br, s, $\nu_{1/2}$ = 860 Hz, 16H, *cy*), 10.52 (br, s, $\nu_{1/2}$ = 930 Hz, 14H, *cy*), 4.8 (br, s, 20H, *cy*), 3.40 (br, s, 21H, *cy*), 2.72 (br, s, 12H, *cy*), 1.44 (br, s, 11H, *cy*); ^{1}H NMR (CD_2Cl_2; 600 MHz, 298 K) δ: 20.31 (br, s, $\nu_{1/2}$ = 2000 Hz, 9H, *cy*), 13.04 (br, s, $\nu_{1/2}$ = 1600 Hz, 18H, *cy*), 10.06 (br, s, $\nu_{1/2}$ = 1800 Hz, 18H, *cy*), 4.71 (s, 20H, *cy*, overlapping with solvent), 3.31 (s, 20H, *cy*), 2.55 (s, 12H, *cy*), 1.18 (s, 10H, *cy*); ^{1}H NMR (CD_2Cl_2; 500 MHz, 187 K)[59] δ: 68.23 (br, s, 3H, *cy*), 46.78 (br, s, 9H, *cy*), 41.45 (br, s 10H, *cy*), 14.55 (br, s, 9H, *cy*), 8.73 (s, 10H, *cy*), 6.64 (s, 11H, *cy*), 2.15 (s, 4H, *cy*) −1.54 (s, 5H, *cy*), −2.06 (s, 6H, *cy*), −11.41 (s, 1H, *cy*), −14.38 (m, 6H, *cy*), −25.25 (br, s, 2H, *cy*); ^{1}H NMR (MeOD-d_4; 600 MHz, 298 K)[60] δ: 4.26, 3.62 (br, s, 27H, *cy*, overlapping with each other and solvent), 2.22 (s, 23H, *cy*), 2.01 (br, s, 31H, *cy*), 1.54 (br, s, 12H, *cy*); ^{1}H NMR (MeOD-d_4; 500 MHz, 187 K) δ: 2.04 (br, m, 9H, *cy*), 1.87 (br, s, 33H, *cy*), 1.76 (br, s, 9H, *cy*), 1.34 (br, m, 42H, *cy*); ^{13}C{^{1}H} NMR (CD_2Cl_2; 151 MHz, 298 K) δ: 58.38 (br, *i-cy*), 38.96 (*cy*), 32.81 (*cy*), 29.95 (*cy*); ^{13}C{^{1}H} NMR (MeOD-d_4; 151 MHz, 298 K) δ: 42.09 ($^{1}J_{CP}$ = 42.1 Hz, *i-cy*), 30.31 (*cy*), 28.84 (*cy*), 27.76 (*cy*); ^{31}P{^{1}H} NMR (CD_2Cl_2; 243 MHz, 298 K) δ: 204.14 (br, s, $\nu_{1/2}$ = 5700 Hz, O*P*), ^{31}P{^{1}H} NMR (CD_2Cl_2; 202 MHz, 187 K) δ: 467.96 (s, 2P, O*P*), 80.92 (s, 1P, O*P*); ^{31}P{^{1}H} NMR (MeOD-d_4; 243 MHz, 298 K) δ: 75.54 (br, s, $\nu_{1/2}$ = 8000 Hz, O*P*), ^{31}P{^{1}H} NMR (MeOD-d_4; 202 MHz, 187 K) δ: 57.14 (s, O*P*). UV/vis/NIR [DCM, λ_{max}, nm (ε, M^{-1} cm^{-1})]: 245.0 (390); [MeOH, λ_{max}, nm (ε, M^{-1} cm^{-1})]: 232.9 (270), 268.5 (30), 446.2 (8) $^{3}P_2$, 470.8 (5) $^{3}P_1$, 483.0 (6) $^{3}P_0$, 595.7 (3) $^{1}D_2$.

$NdBr_3(OPcy_3)_3$

Pale green **$NdBr_3(OPcy_3)_3$** 19 mg, 82%. ^{1}H NMR ($CDCl_3$; 600 MHz, 298 K) δ: 11.77 (br, s, $\nu_{1/2}$ = 590 Hz, 8H, *cy*), 7.39 (br, s, $\nu_{1/2}$ = 320 Hz, 17H, *cy*, overlapping with solvent), 5.53 (br, s, $\nu_{1/2}$ = 400 Hz, 17H, *cy*), 3.05 (br, s, 18H, *cy*), 2.53 (br, s, 19H, *cy*), 2.14 (br, s, $\nu_{1/2}$ = 11H, *cy*), 1.21 (br, s, 11H, *cy*); ^{1}H NMR (CD_2Cl_2; 600 MHz, 298 K) δ: 11.41 (br, s, $\nu_{1/2}$ = 890 Hz, 9H, *cy*), 7.07 (br, s, $\nu_{1/2}$ = 450 Hz, 18H, *cy*), 5.32 (br, s, $\nu_{1/2}$ = 520 Hz, 18H, *cy*, overlapping with solvent), 3.01 (br, s, 18H, *cy*), 2.44 (br, s, 18H, *cy*), 2.07 (br, s, 9H, *cy*), 1.10 (br, m, 9H, *cy*); ^{1}H NMR (CD_2Cl_2; 500 MHz, 187 K) δ: 43.33 (br, s, 6H, *cy*), 28.35 (br, s, 10H, *cy*), 24.11 (br, s, 10H, *cy*), 9.40 (br, s, 10H, *cy*), 5.76, 4.47, 3.64, 2.10, 1.41, 0.55, −0.53 (s, 51H, *cy*, overlapping resonances) −2.76 (br, s, 4H, *cy*), −4.73 (br, s, 6H, *cy*), −6.28 (br, s, 3H, *cy*), −12.34 (br, s, 4H, *cy*); ^{1}H NMR (MeOD-d_4; 600 MHz, 298 K) δ: 2.88 (br, s, $\nu_{1/2}$ = 300 Hz, 18H, *cy*), 2.26 (br, s, $\nu_{1/2}$ = 180 Hz, 18H, *cy*), 1.98 (m, 20H, *cy*), 1.83 (m, 12H, *cy*), 1.63 (br, s, 18H, *cy*), 1.34 (m, 11H, *cy*); ^{1}H NMR (MeOD-d_4; 500 MHz, 187 K) δ: 2.04 (br, m, 9H, *cy*), 1.87 (br, m, 32H, *cy*), 1.75 (br, s, 9H, *cy*), 1.34 (br, m, 41H, *cy*); ^{13}C{^{1}H} NMR (CD_2Cl_2; 151 MHz, 298 K) δ: 44.37 (br, *i-cy*), 33.00 (br, *cy*), 30.81 (*cy*), 28.93 (*cy*); ^{31}P{^{1}H} NMR (CD_2Cl_2; 243 MHz, 298 K) δ: 184.78 (br, s, $\nu_{1/2}$ = 2400 Hz, O*P*), ^{31}P{^{1}H} NMR (CD_2Cl_2; 202 MHz, 187 K) δ: 426.65 (s, 2P, O*P*), 174.66 (s, 1P, O*P*); ^{31}P{^{1}H} NMR (MeOD-d_4; 243 MHz, 298 K) δ: 70.41 (br, s, $\nu_{1/2}$ = 5200 Hz, O*P*), ^{31}P{^{1}H} NMR (MeOD-d_4; 202 MHz, 187 K) δ: 57.12 (s, O*P*). UV/vis/NIR [λ_{max}, nm, single crystal]: 532, 573, 576, 584, 588, 592, 595, 600, 607 – all excitations are $^{4}G_{7/2}$ or $^{4}G_{5/2}$, 738 $^{4}F_{7/2}$, 746(sh) $^{4}S_{3/2}$, 806 $^{2}H_{9/2}$; [DCM, λ_{max}, nm (ε, M^{-1} cm^{-1})]: 531.9 (5), 573.7 (9), 576.3 (sh, 8), 584.6 (8), 587.6 (sh, 7), 606.9 (5) – all

excitations are $^4G_{7/2}$ or $^4G_{5/2}$, 738.2 (4) $^4F_{7/2}$, 747.8 (sh, 4) $^4S_{3/2}$, 806.7 (3) $^2H_{9/2}$; [MeOH, λ_{max}, nm (ε, M^{-1} cm^{-1})]: 217.4 (300), 329.3 (sh, 7) $^2I_{15/2}$ or $^4D_{7/2}$, 349.7 (7) $^2I_{11/2}$, 351.5 (7) $^4D_{1/2}$, 356.5 (7) $^4D_{5/2}$, 429.0 (2) $^2P_{1/2}$, 433.4 (2) $^2P_{1/2}$, 462.4 (sh, 2) $^2K_{15/2}$ or $^4G_{11/2}$, 469.8 (2) $^2D_{3/2}$, 477.3 (2) $^2G_{9/2}$, 512.5 (3) $^4G_{9/2}$ or $^2K_{13/2}$, 524.9 (4) $^4G_{7/2}$, 572.3 (sh, 5) $^4G_{5/2}$ or $^4G_{7/2}$, 583.0 (11) $^4G_{5/2}$ or $^4G_{7/2}$, 626.7 (1) $^2H_{11/2}$, 675.8 (sh, 1) $^4F_{9/2}$, 684.8 (1) $^4F_{9/2}$, 736.1 (5) $^4F_{7/2}$ or $^4S_{3/2}$, 738.7 (5) $^4F_{7/2}$ or $^4S_{3/2}$, 749.1 (9) $^4F_{7/2}$ or $^4S_{3/2}$, 801.0 (14) $^2H_{9/2}$, 866.8 (4) $^4F_{3/2}$, 872.3 (sh, 3) $^4F_{3/2}$, 887.2 (sh, 1) $^4F_{3/2}$.

Results and discussion

Synthesis

Previously published literature on $\mathbf{LnCl_3(OPR_3)_x}$ show that the products have poor solubility or are prone to speciation.[61–63] The more solubilizing bromide anion was studied instead. The known ***mer*-LnBr$_3$(OPcy$_3$)$_3$** (*mer* = meridional; cy = cyclohexyl, C_6H_{11}) have been recently reported and give opportunity for extension to the trivalent actinides, though small lanthanides can speciate.[57,64–66] There has been just one report of a single crystal Am–Br compound, **AmBr$_3$(THF)$_4$**.[67]

The previously reported syntheses of ***mer*-LnBr$_3$(OPcy)$_3$**, (cy = cyclohexyl, C_6H_{11}) utilized boiling ethanol and describe the complexes as having low solubility.[57] By changing the alcohol to iso-propyl alcohol (^{i}PrOH) and working on a scale relevant to actinides, *i.e.* ≤0.02 mmol of metal content, a smooth synthesis is obtained. This was extended to americium by starting from a stock solution of **AmCl$_3$·nH$_2$O** in HCl, precipitating the hydroxide, dissolving the product in $HBr_{(aq)}$ and evaporating to dryness, forming a putative **AmBr$_3$·*n*H$_2$O** solid. Combining the components in ^{i}PrOH initially forms a turbid solution which clarified within minutes and upon standing at room temperature, amber colored X-ray quality crystals formed within 2 h, eqn (2). A small sample was removed for spectroscopy and the solution was left to stand several days to increase the crystalline yield before work up, Fig. 2.

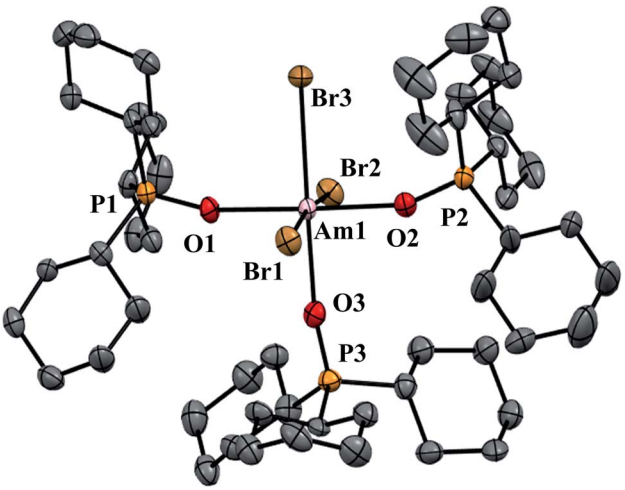

Fig. 2 Thermal ellipsoid plot of AmBr$_3$(OPcy$_3$)$_3$ drawn at the 50% probability level with hydrogen atoms omitted for clarity.

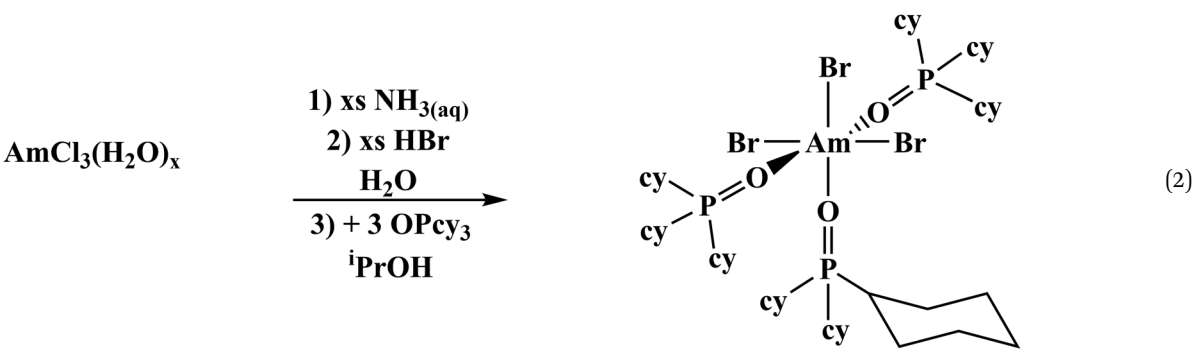

(2)

Crystallography

AmBr$_3$(OPcy$_3$)$_3$ crystallizes as the meridional isomer, ***mer*-AmBr$_3$(OPcy$_3$)$_3$**, in the orthorhombic *Pca*2$_1$ space group and is isomorphous with its lanthanide analogs.[25] Based on the Flack parameter, a small (≤3%) enantiomorphic twin was dealt with using a TWIN/BASF refinement, see ESI.†[68] The Am–Br bond lengths fall into two classes, that of axial (ax) and equatorial (eq) ligands, where axial ligands consist of a homoligand *trans* to the ligand of interest, and equatorial ligands where a hetero ligand is *trans* to the ligand of interest, Fig. 1. The Am–O_{ax} bond lengths are 2.302(7), and 2.312(7) Å while the Am–O_{eq} bond is 2.349(6) Å, a separation of 3σ. The Am–Br_{ax} atoms display a bond distance of 2.870(1), and 2.882(1) Å and the Br_{eq} atom displays a significantly longer distance of 2.912(1) Å. These values are all significantly longer than the 2.8222(6), 2.8445(6), and 2.8610(6) Å bond lengths reported in **AmBr$_3$(THF)$_4$**.[67] However, all of the 2.466(4)–2.533(4) Å Am–O_{THF} bond lengths in **AmBr$_3$(THF)$_4$** are significantly longer than Am–O bond lengths in **AmBr$_3$(OPcy$_3$)$_3$**. The 2.34(1)–2.51(1) Å Am–O bond lengths reported for the **NOPOPO** ligand in **Am(NOPOPO)(NO$_3$)$_3$** and **[Am(NOPOPO)2(NO3)][NO3]2** {**NOPOPO** = Bis[(phosphino)methyl]pyridine-1-oxide, Opy-2,6-$CH_2(Ph)_2PO$} are only comparable to 2.349(6) Å Am–O_{eq} bond since the Am–O_{ax} bond lengths are all significantly shorter, Table 1.[30] All of the X–Am–Y bond angles are between 85.2(2)–95.60(5)° for *cis* ligands and 172.74(3)–178.1(2)° for *trans* ligands, see ESI.†

Table 1 Comparisons of Am–O bond lengths (Å) in selected Am complexes[a]

	Am–OPcy$_{3ax}$	Am-OPcy$_{3eq}$	Am–O$_{NL}$	Am–O$_{PL}$
AmBr$_3$(OPcy$_3$)$_3$	2.302(7), 2.312(7)	2.349(6)		
Am(L)(NO$_3$)$_3$[30]			2.417(9)	2.38(1), 2.39(1)
[Am(L)$_2$(NO$_3$)][NO$_3$]$_2$[30]			2.51(1) 2.506(9)	2.39(1), 2.34(1), 2.38(1), 2.34(1)

[a] L = **NOPOPO**, Opy-2,6-CH$_2$(Ph)$_2$PO.

In the course of preparing the synthesis of ***mer*-AmBr$_3$(OPcy$_3$)$_3$**, the analogous lanthanides, La–Nd, were examined using the modified synthesis stated above, since the 6-coordinate radius of Am^{3+}, 0.975 Å, is most closely related to Nd^{3+}, 0.983 Å.[69] It was found that the Nd and Pr analogs, ***mer*-LnBr$_3$(OPcy$_3$)$_3$**, are isomorphous with the previously reported structures, except the half occupied lattice water was not located in our structures, see ESI.†[57] The Ce analog, ***mer*-CeBr$_3$(OPcy$_3$)$_3$** is not yet reported and the structure was collected. The La analog was reported in the $P2_1$ space group with a lattice ethanol molecule, ***mer*-LaBr$_3$(OPcy$_3$)$_3$·EtOH**, however upon synthesis in ^{i}PrOH, the isomorphous $Pca2_1$ unit cell was obtained and is reported here, see ESI.† Crystals of **CeBr$_3$(OPcy$_3$)$_3$** are orange, while crystals of the La, Pr and Nd analogs are all colorless. Bulk samples of **PrBr$_3$(OPcy$_3$)$_3$** and **NdBr$_3$(OPcy$_3$)$_3$** are pale yellow and pale green, respectively. The bond metrics of the lanthanides examined here all display the same axial/equatorial bonding patterns, that being axial ligands display much shorter bond lengths than equatorial ligands, with distorted octahedral geometries, see ESI.† Additionally, we examined the length of the O=P bond, finding that all of the O=P bond lengths significantly increase from the 1.490(2) Å length reported in the free ligand,[70] The O=P bond length increase in the Am and Ce complexes exhibited an average 0.030 and 0.028 Å, increase, respectively, while the La, Pr and Nd complexes only exhibited a 0.022, 0.023 and 0.022 Å, average bond length increase from the free ligand, respectively.

For the sake of comparison we turned to the d-block to see if the same trend is also observed in transition metals. Two examples, ***mer*-MoCl$_3$(OPMe$_3$)$_3$**[71] and ***mer*-VCl$_3$(OPEt$_3$)$_3$**[72] have been reported. The Mo complex exhibits consistent bond lengths for both the Mo–Cl bonds and the Mo–O bonds. While the V complex shows some evidence of this lengthening of hetero-*trans* ligands where two of the V–Cl bonds are significantly different and two are slightly less than 3σ in separation. The V–O bonds show two bonds that are significantly different and two slightly more than 3σ in separation. We also compared the O=P bond lengths of CoX$_2$(OPcy$_3$)$_2$ (X = Cl, Br, I, NCS) where a regular increase in bond length is observed based on the identity of X, 0.021, 0.018, 0.15 and 0.025 Å, respectively.[73]

Table 2 Inverse-trans-influence calculated from eqn (1) for the MBr$_3$(OPcy$_3$)$_3$ (M = Am, Nd, Pr, Ce, La) series[6]

MBr$_3$(OPcy$_3$)$_3$	Am	Nd	Pr	Ce	La
Radius (Å)[a]	0.975	0.983	0.99	1.01	1.032
ITI$_{M-Br}$	98.8(2)	98.9(2)	98.8(2)	99.0(2)	99.1(1)
ITI$_{M-O}$	98.2(2)	98.6(3)	98.4(2)	98.6(1)	99.0(3)

[a] 6-Coordinate Shannon ionic radius.

With this f-element data in hand, the calculations of ITI effect from eqn (1) were carried out on the **MBr$_3$(OPcy$_3$)$_3$** (M = Am, La, Ce, Pr, Nd) complexes examined here. The data show that a subtle increase in ITI effect is seen with decreasing ionic radius, Table 2, all of the data are within the error of one another. When the ITI calculations were repeated using the crystallographic data for the previously published **LnBr$_3$(OPcy$_3$)$_3$** compounds (Ln = La, Pr, Nd, Gd, Ho), as well as **LnI$_3$(Et$_2$O)$_3$**,[26] **LnCl$_3$(HMPA)$_3$**,[74–76] and the series **YbX$_3$(THF)$_3$** (X = Cl, Br, I),[11,77,78] the data shows no clear trends or patterns with respect to lanthanide or halide identity, where the halide ligands usually show no ITI. The oxygen donors follow the pattern in terms of ITI values where: Et$_2$O > THF > HMPA, which appears counter intuitive since HMPA is regarded as a strong donor, while Et$_2$O is regarded as a weak donor, see Tables S11–S14.† Without more sophisticated investigations and based on these small data sets, it is not clear what ligands affect the values for ITI calculations in terms of donor strength, steric bulk and crystallization effects. No analogous actinide compounds were located, likely due to the prevalence of the +4 oxidation state in the early actinides and the scarcity of *trans*-plutonium crystallographic data.

Electronic absorption spectroscopy

The electronic absorption spectroscopy for **AmBr$_3$(OPcy$_3$)$_3$** shows an intense charge transfer band centered at λ_{max} 340 nm (29 411 cm^{-1}) in addition to the Laporte forbidden 5f → 5f transitions characteristic of Am^{III}.[79,80] With few exceptions, the energies of the absorptions are similar to those reported in the low temperature spectrum of **AmBr$_3$** and the recently reported spectrum of **(PPh$_4$)$_3$AmCl$_6$**.[80,81] The characteristic $^5L_{6'}$ excitation reported at 510 nm (19 588 cm^{-1}) has shifted to 508 nm (19 685 cm^{-1}), Fig. 3.[79,80] All of the transitions were assigned using the reported values for **AmBr$_3$** and were confirmed through theoretical analysis.[79,80] **AmBr$_3$(OPcy$_3$)$_3$** is not fluorescent at room temperature even with long integration times (≥2000 ms) at an excitation wavelength of 365 or 420 nm.

The solid state absorption spectrum of **CeBr$_3$(OPcy$_3$)$_3$** displays an intense charge transfer band with λ_{max} of 339 nm (29 479 cm^{-1}). **NdBr$_3$(OPcy$_3$)$_3$** reveals, sharp hypersensitive transitions of low intensity between 500–607 nm consistent with the $^4G_{7/2}$ and $^4G_{5/2}$ excitations, similar to the values reported for **NdBr$_{3(g)}$** at 1195 °C, while several of the typical 4f → 4f transitions reported for **Nd(ClO$_4$)$_{3(aq)}$** were not observed.[82–84] **LaBr$_3$(OPcy$_3$)$_3$** and **PrBr$_3$(OPcy$_3$)$_3$** gave no UV/vis/NIR peaks

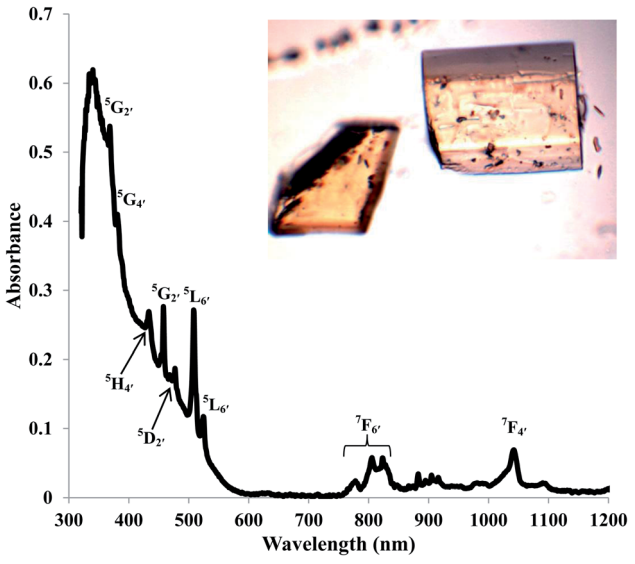

Fig. 3 Solid state UV/vis/NIR of $AmBr_3(OPcy_3)_3$ at room temperature, with excitation assignments and photograph of crystals.

between 320–1700 nm. The former is typical of the $5d^04f^0$ La^{3+} ion, while the latter is unusual for the $4f^2$ Pr^{3+} ion,[84] this may be due to the pseudo inversion center present in $\mathbf{MBr_3(OPcy_3)_3}$. Though the Pr^{3+} ion possesses hypersensitive $^3P_2$ and $^1D_2$ transitions at 444.4 nm (22 500 cm^{-1}) and 588.2 nm (17 000 cm^{-1}), respectively, but were not observed through repeated collections, see Fig. S3–S7† for spectra.[83,84]

To further explore the unusual observations of $\mathbf{PrBr_3(OPcy_3)_3}$, solution phase electronic absorption spectra of all four $\mathbf{LnBr_3(OPcy_3)_3}$ compounds were recorded in a non-coordinating (DCM) and a coordinating (MeOH) solvent. The spectra recorded in DCM reproduce the solid state spectra for all $\mathbf{LnBr_3(OPcy_3)_3}$, with a large charge transfer band observed for $\mathbf{CeBr_3(OPcy_3)_3}$ and the hypersensitive $^4G_{7/2}$ and $^4G_{5/2}$ excitations in Nd being observed. Spectra of $\mathbf{PrBr_3(OPcy_3)_3}$ recorded in DCM display a charge transfer band at λ_{max} 245.0 nm (40 816 cm^{-1}), the edge of which is observed in the other compounds, including the free ligand, see ESI.† The spectra recorded in MeOH told a different story where the $\mathbf{NdBr_3(OPcy_3)_3}$ and $\mathbf{PrBr_3(OPcy_3)_3}$ gave the f → f transitions observed in the respective aquo-ions $\mathbf{Ln(ClO_4)_{3(aq)}}$.[84] With the larger window afforded by MeOH, a large charge transfer band for all the metals in a range of 209–234 nm (47 847–42 735 cm^{-1}), this is also observed in the free ligand and has been characterized as an O=P π → σ* P–C intraligand charge transfer excitation by theoretical analysis. Additionally, $\mathbf{LaBr_3(OPcy_3)_3}$ and $\mathbf{PrBr_3(OPcy_3)_3}$ both display a second, smaller charger transfer peak at 285.5 nm (35 026 cm^{-1}) and 268.5 nm (37 244 cm^{-1}), respectively, which theoretical analysis has characterized as a Br → Ln LMCT excitation. While $\mathbf{CeBr_3(OPcy_3)_3}$ shows several charge transfer peaks 209–315 nm (47 847–31 746 cm^{-1}), see ESI.† None of the lanthanide compounds were fluorescent in the solid state.

Multi-nuclear NMR spectroscopy

In order to gain more insight into the system, and due to the convenient spectroscopic handle provided by the ^{31}P nucleus, ^1H, $^{13}C\{^1H\}$ and $^{31}P\{^1H\}$ multi nuclear NMR spectra were recorded, in a non-coordinating (DCM-d_2) and in a coordinating (MeOD-d_4) solvent, the compounds display limited solubility in alcohols and chloroform, but good solubility in DCM. Due to radiological constraints and small sample sizes obtaining NMR spectra on americium samples can be difficult. Exceptions have included Evans' method studies,[85] a notable solid state MAS study of $\mathbf{AmO_2}$[86] and the recent report of $\mathbf{Am(C_5Me_4H)_3}$.[87] Some $^{31}P\{^1H\}$ data has been reported previously for other $\mathbf{LnBr_3(OPcy_3)_3}$ complexes,[57] here we seek to add to this data and compare it with its americium analog. Because of the weak paramagnetism of the $5f^6$ Am^{3+} ion, 1.64 μ_B,[85] a shorter relaxation time ($d_1 = 1$ s) was utilized along with several extra scans to obtain a good signal for $\mathbf{AmBr_3(OPcy_3)_3}$ at a shift of δ 108.89 ppm, Fig. 4. To the best of our knowledge this is the first report of a ^{31}P NMR signal in an americium complex, however we only able to study the complex in one solvent ($CDCl_3$) due to sample integrity as well as radiological constraints.

The signal of $\mathbf{AmBr_3(OPcy_3)_3}$ is similar in chemical shift to the $4f^1$ $\mathbf{CeBr_3(OPcy_3)_3}$ at δ 109.48 and 107.70 ppm in $CDCl_3$ and CD_2Cl_2, respectively. Both signals are shifted down field from the diamagnetic $\mathbf{LaBr_3(OPcy_3)_3}$ (δ 60.314 and 60.483 ppm in $CDCl_3$ and CD_2Cl_2, respectively) and the free ligand $OPcy_3$ (δ 50.574 ppm, $CDCl_3$) which was recorded for comparison. The more paramagnetic $4f^2$ and $4f^3$ $\mathbf{PrBr_3(OPcy_3)_3}$ and $\mathbf{NdBr_3(OPcy_3)_3}$ are significantly shifted further down field (δ 204.1 and 184.8 ppm, respectively, in CD_2Cl_2) and are significantly broadened ($\nu_{1/2}$ = 5700 and 2400 Hz, respectively), Fig. 4. In the original report of $\mathbf{LnBr_3(OPcy_3)_3}$ it was stated that Nd displays two resonances at δ 187.4 and 167.6 ($CDCl_3$) at room temperature,[57] in our hands both the Pr and Nd gave two signals, however, one is significantly larger than the second and required more than 400 scans to observe, with 800 scans needed for satisfactory signal:noise, see ESI.† We suspect the second resonance is a small phosphorous containing impurity, which was more evident in the variable temperature studies, see

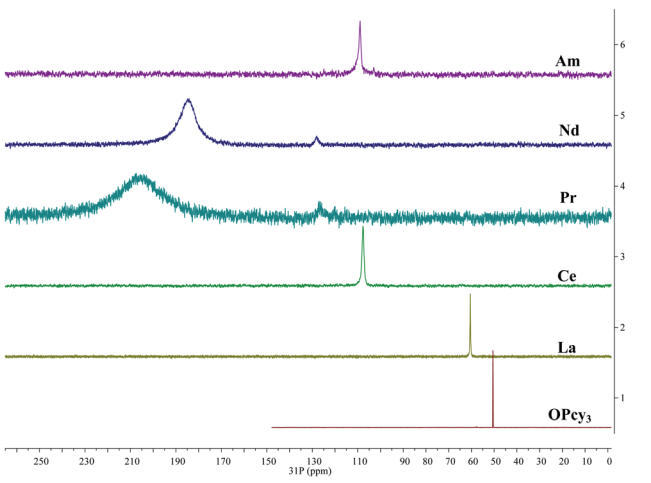

Fig. 4 Stacked $^{31}P\{^1H\}$ NMR spectra of $\mathbf{MBr_3(OPcy_3)_3}$ (M = Am, Nd, Pr, Ce, La) including $OPcy_3$ in $CDCl_3$ or CD_2Cl_2 at 298 K.

below. Due to the high fluxionality of the cyclohexyl rings the ^{1}H NMR spectra are complicated and provide limited information. In particular the paramagnetism in **$PrBr_3(OPcy_3)_3$** and **$NdBr_3(OPcy_3)_3$** give rise to several broad peaks over a range of about 20 ppm, some with widths up to 2000 Hz, see experimental and ESI† for spectra. The $^{13}C\{^{1}H\}$ NMR spectra of **$MBr_3(OPcy_3)_3$** show several signals and are consistent with a single chemical environment for the carbons. Due to the small sample size of **$AmBr_3(OPcy_3)_3$** only three of the expected four signals were observed, with the *ipso*-carbon likely being too broad and weak to be observed in this experiment, though a doublet at δ 27.08 ppm with J_{CP} coupling constant of 27 Hz is consistent with the carbon α to the *ipso*-carbon. For the diamagnetic free ligand and **$LaBr_3(OPcy_3)_3$** both 1-bond and 2-bond C–P coupling was observed with constants of *ca.* 35 and 27 Hz in $CDCl_3$, respectively, see ESI† for spectra. When the same lanthanide complexes were recorded in a coordinating solvent, MeOD-d_4, all of the paramagnetic spectra display smaller paramagnetic shifts for all the observed nuclei relative to their analogous spectra in CD_2Cl_2, see ESI.†

The room temperature $^{31}P\{^{1}H\}$ spectra all display a single resonance at room temperature which contrasts the solid state structures which contain two distinct environments, the short homo-*trans* and the long hetero-*trans* environments, this suggests that the system is highly dynamic at room temperature. To investigate this we recorded low temperature, −86 °C, spectra of all of the lanthanide samples in both MeOD-d_4 and CD_2Cl_2, to ensure all of the $^{31}P\{^{1}H\}$ spectra were quantitative all spectra were recorded with $d_1 \gg T_1$. The spectra of all of the lanthanides in MeOD-d_4 at low temperature all display a single, sharp resonance at δ 57.19 ppm, similar to what would be expected for free $OPcy_3$, see ESI.† It is likely that at low temperature the lanthanide ions shed their phosphine oxide ligands to form the lanthanide bromide solvento complexes.[88] This offers valuable insight into the control of the coordination sphere about the metal atom as different syntheses have shown that product identity is sensitive to the identity of the solvent.[57,89]

It was previously reported that when **$LaBr_3(OPcy_3)_3$** is cooled to −80 °C in CD_2Cl_2 two resonances are observed at δ 62.8 and 62.4 ppm. In our hands when the spectra of **$LnBr_3(OPcy_3)_3$** in CD_2Cl_2 were recorded at −86 °C the La complex gave four signals between δ 62.22 to 60.86 ppm in a 4 : 4 : 2 : 9 ratio. The Ce complex also gave three major resonances between δ 134.28 to 113.90 ppm in a 1 : 3 : 2 ratio, with multiple smaller peaks present, likely due to some decomposition. However the Pr and Nd complexes gave two, well resolved resonances in 2 : 1 ratio at δ 468.0, 80.9 and 426.7, 174.7 ppm, respectively, with a small (<10%) phosphorous containing impurity present that also presents a paramagnetic shift, see ESI.† While not ideal, these results, particularly in CD_2Cl_2 show that at low temperature a static *mer*-octahedral environment is present, similar to the crystal structure, and corroborating earlier studies with these **$LnBr_3(OPcy_3)_3$** complexes.[57,90–92]

Theoretical analysis

Bonding analysis

To obtain a deeper understanding of the bonding in **$MBr_3(OPcy_3)_3$**, a Quantum Theory of Atoms In Molecules (QTAIM) analysis was performed to calculate the concentration of electron density $\rho(r)$, delocalization indices $\delta(r)$, and energy densities [potential, $V(r)$, kinetic, $G(r)$, and total energy densities, $H(r)$]. All of these metrics are utilized to determine the degree of covalency exhibited in the bonding interactions. Based on previous studies where the nature of bonding interactions of f-block complexes has been shown that bonds are not formally covalent, but rather partially covalent.[46,47,93] A partial covalent bond implies positive values for the Laplacian of the electron density, $\nabla\rho(r)$, and negative values for total energy densities, $H(r)$. Here, the term "covalency" refers to the metal–ligand interaction needed to experience orbital overlap, which is reflected by the buildup of electron density [$\rho(r)$] in the interatomic region. Furthermore, covalency can be enhanced by a better energy match between the atomic orbital involved, which is reflected by the delocalization of the electrons in the interatomic region.

From a general perspective the results herein show that the M–Br bonds displays a low concentration of electron density in the

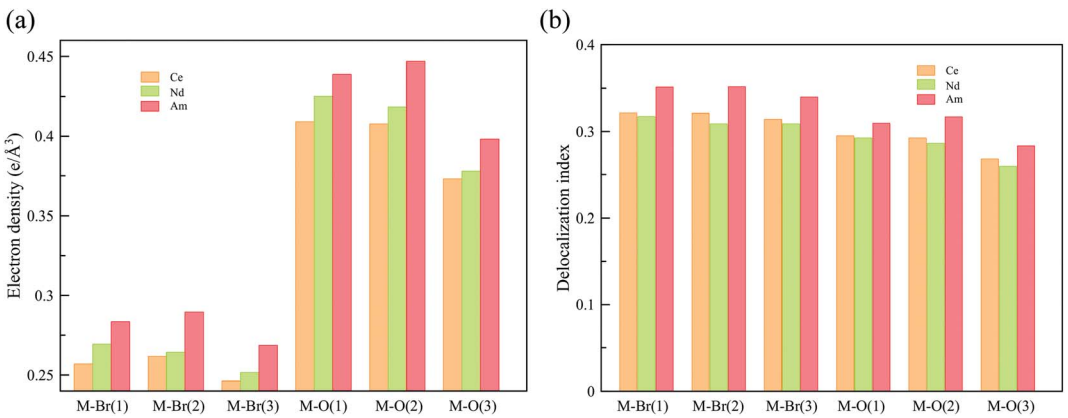

Fig. 5 QTAIM metrics of the Bond Critical Points (BCPs) derived from the SR-CAS(n,7) wave functions, (a) concentration of the electron density, (b) delocalization indices. See ESI† for exact numbers.

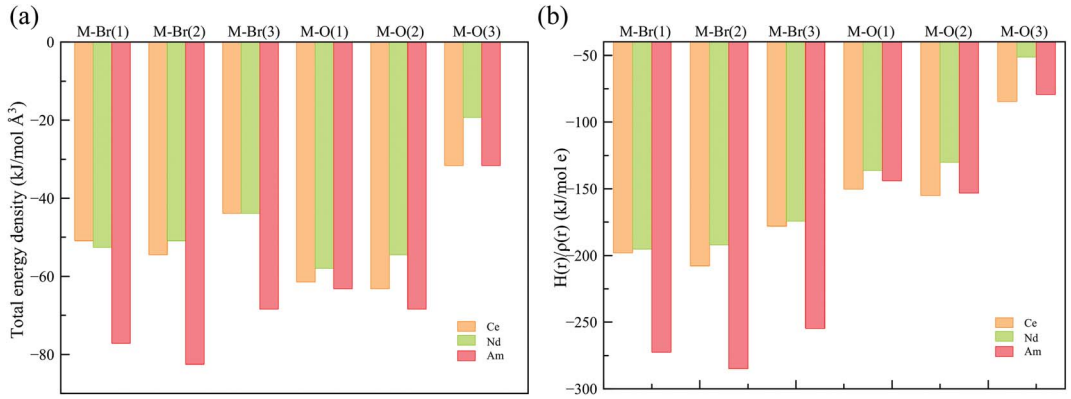

Fig. 6 (a) Total energy density over the electron density (b) total energy density over concentration of electron density at the BCP derived from a SR-CAS(7,7) wave function. See ESI† for exact numbers.

interatomic region compared to the M–O bonds, Fig. 5a, though similar delocalization indices, Fig. 5b, implying that the covalency in the M–O bonds occur due to increased orbital overlap, whereas the better energy match between parent metal–ligand orbitals for the M–Br bonds compensate for the lack of electron density concentration. A more subtle difference is observed in the energy density of the M–O bonds, particularly the M–O(3) bond where $\mathbf{CeBr_3(OPcy_3)_3}$ most resembles $\mathbf{AmBr_3(OPcy_3)_3}$. Whereas the M–Br bonds of $\mathbf{CeBr_3(OPcy_3)_3}$ and $\mathbf{NdBr_3(OPcy_3)_3}$ are closer to each other, Fig. 6a. The origin of these subtleties resides in the balance between kinetic, $G(r)$, and potential energy, $V(r)$, densities with respect to the Laplacian of the electron density, $\nabla^2\rho(r)$, where a more careful treatment can be performed, when the total electron densities, $H(r)$, is normalized by the electron density at the Bond Critical Point (BCP). This allows the role of the kinetic, $G(r)$, and potential energies, $V(r)$, to be isolated from the concentration of electron density, $\rho(r)$, Fig. 6b. When the data are compared, the same trends are observed. It appears that $\mathbf{CeBr_3(OPcy_3)_3}$ and $\mathbf{NdBr_3(OPcy_3)_3}$ differ from each other in that: the bonding patterns are independent of the concentration of electron density, $\rho(r)$, *i.e.* Ce stabilizes the electrons in the interatomic region similarly to Nd when a more polarizable ligand is present like Br, while Ce resembles Am when a harder–donor ligand is present, like OPR_3. Moreover, the dominance of potential energy, $V(r)$, over kinetic energy, $G(r)$ is independent of the electron density, which shows that the covalent contribution in Nd–O(3) bond is almost negligible, Fig. 6b.

Table 3 Ratio between potential [$V(r)$] and kinetic [$G(r)$] energy densities

	$\lvert V(r)\rvert/G(r)$ (kJ mol^{-1} Å^{-3})		
	Ce	Nd	Am
M(1)–Br(1)	1.10	1.10	1.13
M(1)–Br(2)	1.11	1.10	1.14
M(1)–Br(3)	1.09	1.09	1.12
M(1)–O(1)	1.05	1.04	1.04
M(1)–O(2)	1.05	1.04	1.04
M(1)–O(3)	1.03	1.02	1.02

Further characterization of the bonds is provided by the ratio between potential, $V(r)$, and kinetic, $G(r)$, energy densities, that shows the extent of the polarization of the bond, again the M–Br bonds are less polarized than the M–O bonds, where Am shows the least polarized bonds (down to 86% of polarization), Table 3. This agrees with the better energy match provided by Br^- with the lanthanides and actinides, but is most pronounced in the Am complex.

Qualitatively, the ITI correlates with the previous bonding analysis.[27] However, quantitatively, this does not appear to be the case due to the simple shortening of the bond, which could imply different effects operating simultaneously in the complex. Another way to corroborate the presence of the ITI is by the inclusion of the 5/6p orbitals in an all-electron *versus* a frozen-core calculation.[27] Our results show that $\mathbf{CeBr_3(OPcy_3)_3}$ exhibits the highest amount of stabilization (57.9 kJ mol^{-1}), then $\mathbf{AmBr_3(OPcy_3)_3}$ (16.6 kJ mol^{-1}), and $\mathbf{NdBr_3(OPcy_3)_3}$ (11.9 kJ mol^{-1}) shows the least amount of stabilization by the inclusion of the 5/6p shell, which confirms the presence of an ITI-like mechanism in these systems. However, the energies of stabilization do not correlate with the trend observed for the ITI percentages coming directly from the contraction of the bonds in the *trans* positions. This is not necessarily true for a system presenting more than one ITI mechanism because they compete within the same molecule, and therefore become more complicated to analyze. For clarity in the construction of an MO energy level diagram, the cyclohexyl rings were truncated to methyl groups, *e.g.* $\mathbf{MBr_3(OPMe_3)_3}$, Fig. 7.[94] This mixing is produced with the O 2p and P 3s orbitals, providing a more delocalized character of the bond and the stronger mixing between 5p orbitals in Ce is observed, Fig. 7.

Another way to show the role of the Ln/An 5/6p orbitals in an ITI-like mechanism is to assess the reduction of the electron repulsion of these semi-core electrons in the complex with respect to the free-ion. Within ligand field theory (LFT) the one-electron inter-electronic repulsion integrals are described by the Slater–Condon parameters F^k(nl,nl) and the spin–orbit coupling parameter ζ_{nl} (n = shell, l = s, p, d, f).[95,96] Previous studies have successfully applied a non-empirical method to obtain these

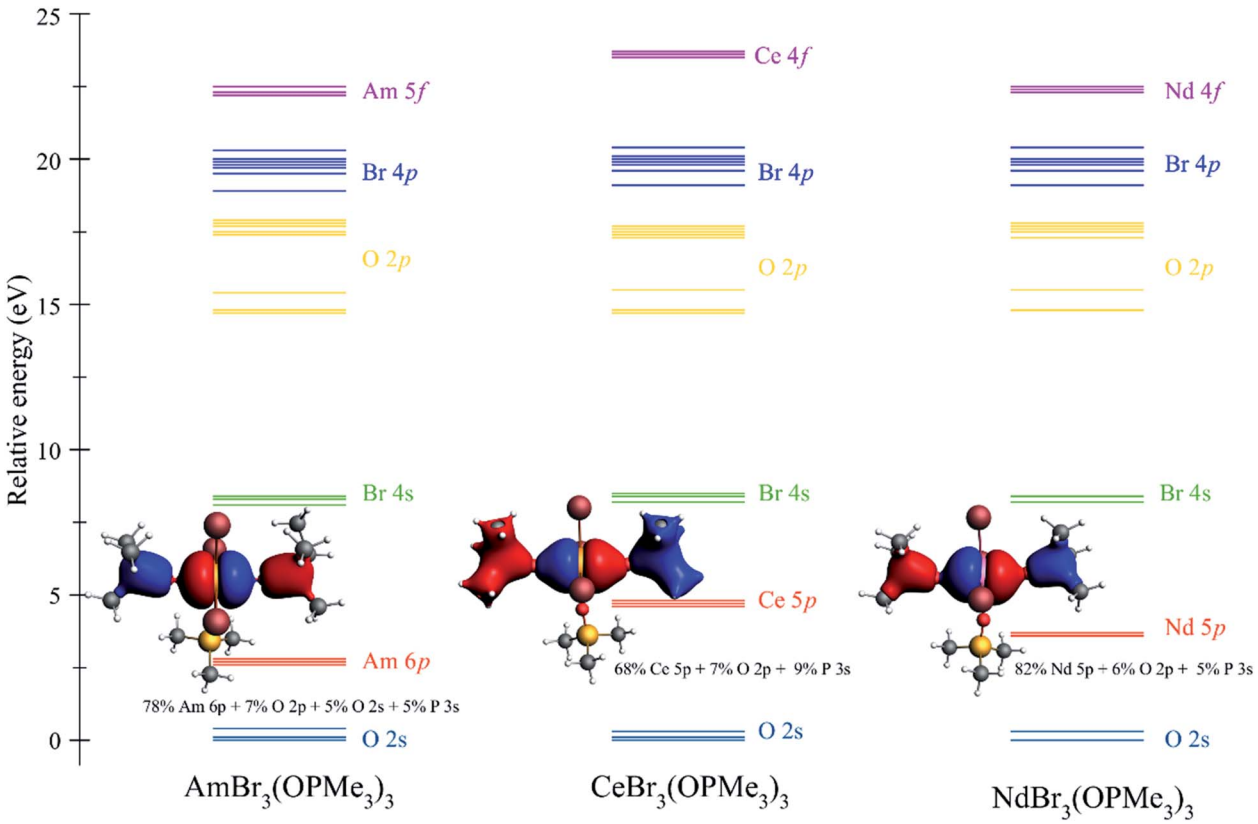

Fig. 7 Molecular orbital (MO) energy level diagram for $MBr_3(OPMe_3)_3$ (M = Am, Ce, Nd) from a scalar relativistic PBE/TZVP calculation. MO labels correspond to the predominant shell in the MO, for the MO composition see Tables S3–S5.† MO depictions correspond to the involvement of the semi-core 5/6p orbitals in orbital mixing.

parameters using a ligand-field DFT (LFDFT) capable of predicting the electronic structure of lanthanide complexes.[52,97–100] Since the reductions of the Slater–Condon parameters with respect to the free-ion are related to the central-field and symmetry-restricted covalency, their evaluation will provide further insight into the nature of an ITI-like mechanism in these complexes.

The reduction of the LF parameters is considerably larger in $CeBr_3(OPcy_3)_3$ compared to $NdBr_3(OPcy_3)_3$ and $AmBr_3(OPcy_3)_3$, whose reductions are similar, Table 4. These results agree with the stabilization energies obtained between frozen-core to all-electron calculations, confirming the presence of an ITI-like mechanism. This also shows that the sizable reductions indicate an important covalent component related to the 5/6p orbital involvement in the interaction between the metal ions and the Br^- and phosphine oxide ligands.

The differences in bonding observed between lanthanides and actinides make the comparison more complicated due to the involvement of the 5f electrons in the case of americium, which significantly increases the covalent character of the bond. In this context, only Ce and Nd could be compared with QTAIM metrics, where delocalization and total energy densities predict the trend observed in the stabilization energies from the involvement of the 5p electrons.

Further insight into the nature of metal–ligand bonding and the role of pseudo-core orbitals can be obtained by localizing the electron density through natural localized molecular orbitals (NLMOs). Assuming these systems behave as Lewis

Table 4 Reduction of the Slater–Condon parameters[a] of 5/6p semi-core electrons derived from LF-DFT

	F^2(p,p) (eV)			$\zeta_{5/6p}$ (eV)		
	$[M(H_2O)_9]^{3+}$	$MBr_3(OPcy)_3$	Δ_{red}[b]	$[M(H_2O)_9]^{3+}$	$MBr_3(OPcy)_3$	Δ_{red}[b]
Ce^{III}	28%	70%	42%	18%	47%	29%
Nd^{III}	21%	43%	22%	15%	28%	13%
Am^{III}	19%	45%	25%	14%	27%	12%

[a] See ESI for Slater–Condon parameters. [b] Δ_{red} refers to the difference between the aquo and $MBr_3(OPcy)_3$ (M = Ce, Nd, Am) complexes.

structures, NLMOs provide a good alternative to understand the nature of the bonds.

In order to confirm the involvement of pseudo-core electrons in this ITI-like mechanism, the uranyl unit $[UO_2]^{2+}$ was calculated as a reference sample, as it corresponds to the strongest known example of the ITI.[10] Within the NLMO framework, the 6s and 6p pseudo-core electrons deviate from the core behavior, especially one p orbital that by symmetry can mix with the oxo 2p orbitals. This NLMO is dominated by a uranium pf natural hybrid orbital (NHO) (76% 6p + 24% 5f) with polarization towards the oxo ligands, Table S7.† A similar picture is seen in the theoretical models $\mathbf{MBr_3(OPMe_3)_3}$ (M = Am, Nd), where the pseudo-core electrons are delocalized with 4f/5f orbitals and display some polarization towards the O and P atoms of the phosphine oxide ligands, with the Am analog the most similar to U in terms of hybridization. The Ce analog shows a slightly different pattern, where pf hybridization is rather small and orbital mixing is produced directly between pseudo-core electrons and the phosphine oxide ligands, NLMOs 4–5, Table S7.† This implies that the bonds in Ce should be more directional than in the Am and Nd analogs.

Moving strictly to the nature of the bond, all three have similar bonding patterns, although Am shows a more balanced 5f/6d ratio in the formation of NLMOs, see Tables S8–S10.† This is somewhat expected in that bond formation in trivalent lanthanide complexes is primarily through 5d orbitals. The M–$OPcy_3$ bonds are formed by involvement of orbitals from the phosphine oxide moiety giving rise to highly polarized covalent bonds. On the other hand, the M–Br bonds are less polar because of the better energy match between the 4p orbitals and the 4f/5f metal orbitals. This could also be related to what is observed in the QTAIM results, where the M–Br bonds are as delocalized as the M–$OPcy_3$ bonds but with a lower concentration of electron density, see ESI.†

Based on the above results, we can describe the bonding in these $\mathbf{LnBr_3(OPcy_3)_3}$ molecules as displaying an ITI effect because the pseudo-core electrons are delocalized only towards the f orbitals in the same way as for the uranyl unit. The involvement of the f and d orbitals remains very close to what is expected for trivalent complexes.

Conclusions

The synthesis and characterization of $\mathbf{AmBr_3(OPcy_3)_3}$ has been achieved and shows the same meridional coordination geometry as the larger lanthanides. Spectroscopic analysis by single crystal X-ray diffraction shows that the homo-*trans* ligands display significantly shorter bonds than the hetero-*trans* ligands. Single crystal UV/vis/NIR spectra show large charge transfer bands for the Ce and Am complexes. Analysis by ^{31}P NMR spectroscopy illustrates the weak paramagnetism of the $5f^6$ Am^{3+} center. Bonding analyses show that the complex displays a significant inverse-trans-influence (ITI) with the bonding ligands, though its mechanism is not directly related to the involvement of the 5/6p electrons. This suggests that there is interplay between the involvement of valence electrons that significantly separates the lanthanides from the actinides. $\mathbf{CeBr_3(OPcy_3)_3}$ shows the highest amount of 5p electron involvement in covalency. This is observed by the reduction of the electron–electron repulsion of the 5p shell compared to the aquo-complex, $\mathbf{[Ce(H_2O)_9]^{3+}}$. This study provides further evidence of an ITI-like mechanism in low-valent f-block complexes, and their potential occurrence in heavier actinides, whose chemistry is dominated by the trivalent oxidation state. Furthermore, it constitutes a new feature that can be exploited for rational ligand design in order to achieve selective ligands for separations in nuclear waste treatment.

Conflicts of interest

The authors declare no competing financial interest.

Acknowledgements

We thank the support of the U.S. Department of Energy, Office of Science, Office of Basic Energy Sciences, Heavy Element Chemistry program under Award Number DE-FG02-13ER16414. The ^{243}Am used in this research were supplied by the U.S. Department of Energy Isotope Program, managed by the Office of Science for Nuclear Physics. We thank Dr Benjamin W. Stein and Dr Conrad A. P. Goodwin of Los Alamos National Laboratory for helpful discussions. We are grateful to Dr Ion Ghiviriga, Prof. Adam Veige, and Dr Banghao Chen for their assistance with the NMR experiments as well as Dr Xinsong Lin for his assistance with the DART-MS. We thank Mr Jason Johnson and Ms Ashley Gray of Florida State University for radiological assistance.

Notes and references

1 V. V. Grushin, *Chem. Rev.*, 2004, **104**, 1629–1662.
2 E. K. Watson and W. A. Rickelton, *Solvent Extr. Ion Exch.*, 1992, **10**, 879–889.
3 F. Arnaud-Neu, J. K. Browne, D. Byrne, D. J. Marrs, M. A. McKervey, P. O'Hagan, M. J. Schwing-Weill and A. Walker, *Chem.–Eur. J.*, 1999, **5**, 175–186.
4 M. Gilmore, É. N. McCourt, F. Connolly, P. Nockemann, M. Swadźba-Kwaśny and J. D. Holbrey, *ACS Sustainable Chem. Eng.*, 2018, **6**, 17323–17332.
5 L. R. Morss, N. M. Edelstein and J. Fuger, *The Chemistry of the Actinide and Transactinide Elements*, Springer, Dordrecht, The Netherlands, 4th edn, 2010.
6 S. Mishra, *Coord. Chem. Rev.*, 2008, **252**, 1996–2025.
7 C. Berthon, N. Boubals, I. A. Charushnikova, D. Collison, S. M. Cornet, C. Den Auwer, A. J. Gaunt, N. Kaltsoyannis, I. May, S. Petit, M. P. Redmond, S. D. Reilly and B. L. Scott, *Inorg. Chem.*, 2010, **49**, 9554–9562.
8 M. B. Jones and A. J. Gaunt, *Chem. Rev.*, 2013, **113**, 1137–1198.
9 A. W. G. Platt, *Coord. Chem. Rev.*, 2017, **340**, 62–78.
10 R. G. Denning, *J. Phys. Chem. A*, 2007, **111**, 4125–4143.
11 T. J. Emge, A. Kornienko and J. G. Brennan, *Acta Crystallogr., Sect. C: Struct. Chem.*, 2009, **65**, m422–m425.

12 K. Krogh-Jespersen, M. D. Romanelli, J. H. Melman, T. J. Emge and J. G. Brennan, *Inorg. Chem.*, 2010, **49**, 552–560.

13 A. J. Lewis, K. C. Mullane, E. Nakamaru-Ogiso, P. J. Carroll and E. J. Schelter, *Inorg. Chem.*, 2014, **53**, 6944–6953.

14 H. S. La Pierre, M. Rosenzweig, B. Kosog, C. Hauser, F. W. Heinemann, S. T. Liddle and K. Meyer, *Chem. Commun.*, 2015, **51**, 16671–16674.

15 M. Gregson, E. Lu, D. P. Mills, F. Tuna, E. J. McInnes, C. Hennig, A. C. Scheinost, J. McMaster, W. Lewis, A. J. Blake, A. Kerridge and S. T. Liddle, *Nat. Commun.*, 2017, **8**, 14137.

16 I. Fryer-Kanssen and A. Kerridge, *Chem. Commun.*, 2018, **54**, 9761–9764.

17 E. Lu, S. Sajjad, V. E. J. Berryman, A. J. Wooles, N. Kaltsoyannis and S. T. Liddle, *Nat. Commun.*, 2019, **10**, 634.

18 D. Brown and C. E. F. Rickard, *J. Chem. Soc. A*, 1971, 81–87.

19 K. W. Bagnall, J. G. H. du Preez, B. J. Gellatly and J. H. Holloway, *Dalton Trans.*, 1975, 1963–1968.

20 B. J. Coe and S. J. Glenwright, *Coord. Chem. Rev.*, 2000, **203**, 5–80.

21 A. J. Lewis, P. J. Carroll and E. J. Schelter, *J. Am. Chem. Soc.*, 2013, **135**, 13185–13192.

22 B. Kosog, H. S. La Pierre, F. W. Heinemann, S. T. Liddle and K. Meyer, *J. Am. Chem. Soc.*, 2012, **134**, 5284–5289.

23 S. G. Minasian, J. M. Keith, E. R. Batista, K. S. Boland, D. L. Clark, S. D. Conradson, S. A. Kozimor, R. L. Martin, D. E. Schwarz, D. K. Shuh, G. L. Wagner, M. P. Wilkerson, L. E. Wolfsberg and P. Yang, *J. Am. Chem. Soc.*, 2012, **134**, 5586–5597.

24 H. S. La Pierre and K. Meyer, *Inorg. Chem.*, 2013, **52**, 529–539.

25 L. P. Spencer, P. Yang, S. G. Minasian, R. E. Jilek, E. R. Batista, K. S. Boland, J. M. Boncella, S. D. Conradson, D. L. Clark, T. W. Hayton, S. A. Kozimor, R. L. Martin, M. M. MacInnes, A. C. Olson, B. L. Scott, D. K. Shuh and M. P. Wilkerson, *J. Am. Chem. Soc.*, 2013, **135**, 2279–2290.

26 T. P. Gompa, N. T. Rice, D. R. Russo, L. M. Aguirre Quintana, B. J. Yik, J. Bacsa and H. S. La Pierre, *Dalton Trans.*, 2019, **48**, 8030–8033.

27 E. O'Grady and N. Kaltsoyannis, *Dalton Trans.*, 2002, 1233–1239.

28 R. G. Denning, in *Complexes, Clusters and Crystal Chemistry*, Springer Berlin Heidelberg, Berlin, Heidelberg, 1992, pp. 215–276.

29 P. I. Matveev, N. E. Borisova, N. G. Andreadi, G. G. Zakirova, V. G. Petrov, E. V. Belova, S. N. Kalmykov and B. F. Myasoedov, *Dalton Trans.*, 2019, **48**, 2554–2559.

30 J. F. Corbey, B. M. Rapko, Z. Wang, B. K. McNamara, R. G. Surbella III, K. L. Pellegrini and J. M. Schwantes, *Inorg. Chem.*, 2018, **57**, 2278–2287.

31 J. N. Cross, J. A. Macor, J. A. Bertke, M. G. Ferrier, G. S. Girolami, S. A. Kozimor, J. R. Maassen, B. L. Scott, D. K. Shuh, B. W. Stein and S. C. Stieber, *Angew. Chem., Int. Ed.*, 2016, **55**, 12755–12759.

32 *APEX3, 2017, 3–0*, Bruker AXS, Inc., Madison, WI, 2017.

33 *SAINT, 8.34a*, Bruker AXS, Inc, Madison, WI, 2013.

34 G. M. Sheldrick, *SADABS, 2012/1*, Bruker AXS, Inc, Madison, WI, 2012.

35 G. M. Sheldrick, *Acta Crystallogr., Sect. A: Found. Adv.*, 2015, **71**, 3–8.

36 G. M. Sheldrick, *Acta Crystallogr., Sect. C: Struct. Chem.*, 2015, **71**, 3–8.

37 O. V. Dolomanov, L. J. Bourhis, R. J. Gildea, J. A. K. Howard and H. Puschmann, *J. Appl. Crystallogr.*, 2009, **42**, 339–341.

38 P.-Å. Malmqvist and B. O. Roos, *Chem. Phys. Lett.*, 1989, **155**, 189–194.

39 F. Neese, *Wiley Interdiscip. Rev.: Comput. Mol. Sci.*, 2018, **8**, e1327.

40 N. Kaltsoyannis, *Inorg. Chem.*, 2013, **52**, 3407–3413.

41 Q. R. Huang, J. R. Kingham and N. Kaltsoyannis, *Dalton Trans.*, 2015, **44**, 2554–2566.

42 I. Fryer-Kanssen, J. Austin and A. Kerridge, *Inorg. Chem.*, 2016, **55**, 10034–10042.

43 A. Kerridge, *Chem. Commun.*, 2017, **53**, 6685–6695.

44 F. D. White, A. N. Gaiser, E. J. Warzecha, J. M. Sperling, C. Celis-Barros, S. R. Salpage, Y. Zhou, T. Dilbeck, A. J. Bretton, D. S. Meeker, K. G. Hanson and T. E. Albrecht-Schmitt, *Inorg. Chem.*, 2018, **57**, 12969–12975.

45 B. E. Klamm, C. J. Windorff, C. Celis-Barros, M. L. Marsh, D. S. Meeker and T. E. Albrecht-Schmitt, *Inorg. Chem.*, 2018, **57**, 15389–15398.

46 E. Warzecha, C. Celis-Barros, T. Dilbeck, K. Hanson and T. E. Albrecht-Schmitt, *Inorg. Chem.*, 2019, **58**, 228–233.

47 A. T. Chemey, C. Celis-Barros, K. Huang, J. M. Sperling, C. J. Windorff, R. E. Baumbach, D. E. Graf, D. Páez-Hernández, M. Ruf, D. E. Hobart and T. E. Albrecht-Schmitt, *Inorg. Chem.*, 2019, **58**, 637–647.

48 D. Dan, C. Celis-Barros, F. D. White, J. M. Sperling and T. E. Albrecht-Schmitt, *Chem.–Eur. J.*, 2019, **25**, 3248–3252.

49 E. Espinosa, I. Alkorta, J. Elguero and E. Molins, *J. Chem. Phys.*, 2002, **117**, 5529–5542.

50 G. te Velde, F. M. Bickelhaupt, E. J. Baerends, C. Fonseca Guerra, S. J. A. van Gisbergen, J. G. Snijders and T. Ziegler, *J. Comput. Chem.*, 2001, **22**, 931–967.

51 C. Fonseca Guerra, J. G. Snijders, G. te Velde and E. J. Baerends, *Theor. Chem. Acc.*, 1998, **99**, 391–403.

52 H. Ramanantoanina, W. Urland, F. Cimpoesu and C. Daul, *Phys. Chem. Chem. Phys.*, 2013, **15**, 13902–13910.

53 M. Atanasov, C. A. Daul and C. Rauzy, in *Optical Spectra and Chemical Bonding in Inorganic Compounds: Special Volume dedicated to Professor Jørgensen I*, ed. D. M. P. Mingos and T. Schönherr, Springer Berlin Heidelberg, Berlin, Heidelberg, 2004, pp. 97–125.

54 P. Lindqvist-Reis, C. Apostolidis, J. Rebizant, A. Morgenstern, R. Klenze, O. Walter, T. Fanghänel and R. G. Haire, *Angew. Chem., Int. Ed.*, 2007, **46**, 919–922.

55 R. E. Gerkin and W. J. Reppart, *Acta Crystallogr., Sect. C: Cryst. Struct. Commun.*, 1984, **40**, 781–786.

56 Y. V. Nelyubina, L. N. Puntus and K. A. Lyssenko, *Chem.–Eur. J.*, 2014, 2860–2865.

57 A. Bowden, A. M. J. Lees and A. W. G. Platt, *Polyhedron*, 2015, **91**, 110–119.
58 Because all of the signals are overlapping no meaningful integration can be obtained, therefore only peaks are listed, see ESI† for spectrum.
59 Due to the numerous peaks only relative integrations are given.
60 Due to the breadth of the peaks only tentative integrations are given.
61 J. V. Kingston, E. M. Krankovits and R. J. Magee, *Inorg. Nucl. Chem. Lett.*, 1969, **5**, 485–489.
62 M. J. Glazier, W. Levason, M. L. Matthews, P. L. Thornton and M. Webster, *Inorg. Chim. Acta*, 2004, **357**, 1083–1091.
63 N. J. Hill, W. Levason, M. C. Popham, G. Reid and M. Webster, *Polyhedron*, 2002, **21**, 445–455.
64 A. M. J. Lees and A. W. G. Platt, *Polyhedron*, 2014, **67**, 368–372.
65 Y. C. Chen, J. L. Liu, L. Ungur, J. Liu, Q. W. Li, L. F. Wang, Z. P. Ni, L. F. Chibotaru, X. M. Chen and M. L. Tong, *J. Am. Chem. Soc.*, 2016, **138**, 2829–2837.
66 Y. X. Wang, Y. Ma, Y. Chai, W. Shi, Y. Sun and P. Cheng, *J. Am. Chem. Soc.*, 2018, **140**, 7795–7798.
67 S. S. Galley, J. M. Sperling, C. J. Windorff, M. Zeller, T. E. Albrecht-Schmitt and S. C. Bart, *Organometallics*, 2019, **38**, 606–609.
68 H. Flack, *Acta Crystallogr., Sect. A: Found. Crystallogr.*, 1983, **39**, 876–881.
69 R. Shannon, *Acta Crystallogr., Sect. A: Cryst. Phys., Diffr., Theor. Gen. Crystallogr.*, 1976, **32**, 751–767.
70 J. A. Davies, S. Dutremez and A. A. Pinkerton, *Inorg. Chem.*, 1991, **30**, 2380–2387.
71 F. A. Cotton and R. L. Luck, *Acta Crystallogr., Sect. C: Cryst. Struct. Commun.*, 1991, **47**, 1069–1072.
72 F. A. Cotton, J. Lu and T. Ren, *Inorg. Chim. Acta*, 1994, **215**, 47–54.
73 R. Bou-Moreno, S. A. Cotton, V. Hunter, K. Leonard, A. W. G. Platt, P. R. Raithby and S. Schiffers, *Polyhedron*, 2011, **30**, 2832–2836.
74 L. J. Radonovich and M. D. Glick, *J. Inorg. Nucl. Chem.*, 1973, **35**, 2745–2752.
75 X.-W. Zhang, X.-F. Li, F. Benetollo and G. Bombieri, *Inorg. Chim. Acta*, 1987, **139**, 103–104.
76 Z. Hou, K. Kobayashi and H. Yamazaki, *Chem. Lett.*, 1991, **20**, 265–268.
77 G. B. Deacon, T. Feng, P. C. Junk, B. W. Skelton, A. N. Sobolev and A. H. White, *Aust. J. Chem.*, 1998, **51**, 75–89.
78 G. B. Deacon, T. Feng, P. C. Junk, G. Meyer, N. M. Scott, B. W. Skelton and A. H. White, *Aust. J. Chem.*, 2000, **53**, 853–865.
79 W. T. Carnall and B. G. Wybourne, *J. Chem. Phys.*, 1964, **40**, 3428–3433.
80 R. G. Pappalardo, W. T. Carnall and P. R. Fields, *J. Chem. Phys.*, 1969, **51**, 1182–1200.
81 J. N. Cross, J. Su, E. R. Batista, S. K. Cary, W. J. Evans, S. A. Kozimor, V. Mocko, B. L. Scott, B. W. Stein, C. J. Windorff and P. Yang, *J. Am. Chem. Soc.*, 2017, **139**, 8667–8677.
82 B. R. Judd, *J. Chem. Phys.*, 1966, **44**, 839–840.
83 D. E. Henrie, R. L. Fellows and G. R. Choppin, *Coord. Chem. Rev.*, 1976, **18**, 199–224.
84 K. Binnemans and C. Görller-Walrand, *Chem. Phys. Lett.*, 1995, **235**, 163–174.
85 T. F. Wall, S. Jan, M. Autillo, K. L. Nash, L. Guerin, C. L. Naour, P. Moisy and C. Berthon, *Inorg. Chem.*, 2014, **53**, 2450–2459.
86 L. Martel, N. Magnani, J. F. Vigier, J. Boshoven, C. Selfslag, I. Farnan, J. C. Griveau, J. Somers and T. Fanghänel, *Inorg. Chem.*, 2014, **53**, 6928–6933.
87 C. A. P. Goodwin, J. Su, T. E. Albrecht-Schmitt, A. V. Blake, E. R. Batista, S. R. Daly, S. Dehnen, W. J. Evans, A. J. Gaunt, S. A. Kozimor, N. Lichtenberger, B. L. Scott and P. Yang, *Angew. Chem., Int. Ed.*, 2019, **58**, 11695–11699.
88 Since the MeOD-d_4 was not rigorously dried, there is water present in all of the spectra leaving the possibility to form complex $Ln(H_2O)_x(MeOD)_yBr_3$ compounds where Br can be inner or outer sphere.
89 A. Bowden, A. W. G. Platt, K. Singh and R. Townsend, *Inorg. Chim. Acta*, 2010, **363**, 243–249.
90 A. Bowden, S. J. Coles, M. B. Pitak and A. W. Platt, *Inorg. Chem.*, 2012, **51**, 4379–4389.
91 A. Bowden, S. J. Coles, M. B. Pitak and A. W. G. Platt, *Polyhedron*, 2014, **68**, 258–264.
92 S. J. Coles, M. B. Pitak and A. W. G. Platt, *Eur. J. Inorg. Chem.*, 2017, **2017**, 1464–1471.
93 C. Celis-Barros, D. Páez-Hernández, M. J. Beltrán-Leiva and R. Arratia-Perez, *Phys. Chem. Chem. Phys.*, 2018, **20**, 4038–4049.
94 The truncated molecules were utilized to remove C–C and C–H interactions of similar energy from the MO calculations, calculations on the metal–ligand interactions were shown to be the same on the full and truncated molecules, see theoretical details in the experimental section and the ESI for further details.†
95 A. B. P. Lever, *Inorganic electronic spectroscopy*, Elsevier Pub. Co, Amsterdam, New York, 1968.
96 E. U. Condon and G. Shortley, *The theory of atomic spectra*, Cambridge University Press, Cambridge, 1951.
97 H. Ramanantoanina, W. Urland, B. Herden, F. Cimpoesu and C. Daul, *Phys. Chem. Chem. Phys.*, 2015, **17**, 9116–9125.
98 H. Ramanantoanina, M. Sahnoun, A. Barbiero, M. Ferbinteanu and F. Cimpoesu, *Phys. Chem. Chem. Phys.*, 2015, **17**, 18547–18557.
99 H. Ramanantoanina, W. Urland, A. García-Fuente, F. Cimpoesu and C. Daul, *Chem. Phys. Lett.*, 2013, **588**, 260–266.
100 H. Ramanantoanina, F. Cimpoesu, C. Göttel, M. Sahnoun, B. Herden, M. Suta, C. Wickleder, W. Urland and C. Daul, *Inorg. Chem.*, 2015, **54**, 8319–8326.

